World Journal of Gastroenterology

Submit a Manuscript: http://www.wjgnet.com/esps/ *World J Gastroenterol* 2017 March 21; 23(11): 1990-2001

DOI: 10.3748/wjg.v23.i11.1990 ISSN 1007-9327 (print) ISSN 2219-2840 (online)

ORIGINAL ARTICLE

Basic Study

Chemotherapy response evaluation in a mouse model of gastric cancer using intravoxel incoherent motion diffusion-weighted MRI and histopathology

Jin Cheng, Yi Wang, Chun-Fang Zhang, He Wang, Wei-Zhen Wu, Feng Pan, Nan Hong, Jie Deng

Jin Cheng, Yi Wang, Wei-Zhen Wu, Feng Pan, Nan Hong, Department of Radiology, Peking University People's Hospital, Beijing 100044, China

Chun-Fang Zhang, Clinical Epidemiology and Medical Statistics, Peking University People's Hospital, Beijing 100044, China

He Wang, GE Healthcare, Shanghai 200050, China

Jie Deng, Department of Medical Imaging, Ann and Robert H. Lurie Children's Hospital of Chicago, Department of Radiology, Feinberg School of Medicine, Northwestern University, Chicago, IL 60611-2605, United States

Author contributions: Cheng J performed the animal experiments, reviewed the experimental and histological data, and wrote the manuscript; Wang Y designed the entire scientific research, instructed manuscript writing, and revised the manuscript; Zhang CF instructed the statistical analysis; Wang H adjusted the parameters of IVIM-DWI scanning; Wu WZ performed the animal experiments and recorded the experimental data; Pan F performed the animal experiments and recorded the experimental data; Hong N instructed the animal experiments and revised the manuscript; Deng J wrote the Metlab program of the bi-exponential IVIM model and analyzed the IVIM parameter data.

Institutional review board statement: The study was reviewed and approved by the Peking University People's Hospital Institutional Review Board.

Institutional animal care and use committee statement: All procedures involving animals were reviewed and approved by the Institutional Animal Care and Use Committee of the Peking University People's Hospital (IACUC protocol number: 2013-0010).

Conflict-of-interest statement: All authors declared that there was no conflict of interest related to this study.

Data sharing statement: Technical appendix, statistical code, and dataset are available from the corresponding author at wangyi@pkuph.edu.cn. Participants gave informed consent for data sharing.

Manuscript source: Unsolicited manuscript

Correspondence to: Yi Wang, MD, Department of Radiology, Peking University People's Hospital, 11 Xizhimen South St., Beijing 100044, China. wangyi@pkuph.edu.cn
Telephone: +86-10-88325813
Fax: +86-10-68318386

Received: December 22, 2016
Peer-review started: December 23, 2016
First decision: January 10, 2017
Revised: January 19, 2017
Accepted: February 17, 2017
Article in press: February 17, 2017
Published online: March 21, 2017

Abstract

AIM

To determine the role of intravoxel incoherent motion (IVIM) diffusion-weighted (DW) magnetic resonance imaging (MRI) using a bi-exponential model in chemotherapy response evaluation in a gastric cancer mouse model.

METHODS

Mice bearing MKN-45 human gastric adenocarcinoma xenografts were divided into four treated groups (TG1, 2, 3 and 4, n = 5 in each group) which received Fluorouracil and Calcium Folinate and a control group (CG, n = 7). DW-MRI scans with 14 b-values (0-1500 s/mm^2) were performed before and after treatment on days 3, 7, 14 and 21. Fast diffusion component (presumably pseudo-perfusion) parameters including the fast diffusion coefficient (D*) and fraction volume (f_p), slow diffusion coefficient (D) and the conventional apparent diffusion coefficients (ADC) were calculated by fitting the IVIM model to the measured DW signals. The median changes from the baseline to each post-treatment time point for each measurement (ΔADC, ΔD* and Δf_p) were calculated. The differences in the median changes between the two groups were compared using the mixed linear regression model by the restricted maximum likelihood method shown as z values. Histopathological analyses including Ki-67, CD31, TUNEL and H&E were conducted in conjunction with the MRI scans. The median percentage changes were compared with the histopathological analyses between the pre- and post-treatment for each measurement.

RESULTS

Compared with the control group, D* in the treated group decreased significantly (ΔD*$_{treated}$% = -30%, -34% and -20%, with z = -5.40, -4.18 and -1.95. P = 0.0001, 0.0001 and 0.0244) and f_p increased significantly (Δ$f_{ptreated}$% = 93%, 113% and 181%, with z = 4.63, 5.52, and 2.12, P = 0.001, 0.0001 and 0.0336) on day 3, 7 and 14, respectively. Increases in ADC in the treated group were higher than those in the control group on days 3 and 14 (z = 2.44 and 2.40, P = 0.0147 and P = 0.0164).

CONCLUSION

Fast diffusion measurements derived from the bi-exponential IVIM model may be more sensitive imaging biomarkers than ADC to assess chemotherapy response in gastric adenocarcinoma.

Key words: Xenografts; Intravoxel incoherent diffusion-weighted magnetic resonance imaging; Chemotherapy; Treatment response; Gastric adenocarcinoma

Core tip: In a mouse gastric cancer model, we demonstrated that the intravoxel incoherent motion (IVIM)-derived tissue perfusion coefficient (D*) decreased, whereas perfusion fraction (PF) increased immediately after chemotherapy and during the treatment course. No considerable overlaps were observed in D* and PF measurements between the treated and control groups. IVIM-derived perfusion measurements offer a potential accurate evaluation of chemotherapeutic efficacy. This imaging study is ready to be translated into a clinical study and may facilitate individualized treatment strategy and prompt treatment adjustment in gastric cancer patients.

Cheng J, Wang Y, Zhang CF, Wang H, Wu WZ, Pan F, Hong N, Deng J. Chemotherapy response evaluation in a mouse model of gastric cancer using intravoxel incoherent motion diffusion-weighted MRI and histopathology. *World J Gastroenterol* 2017; 23(11): 1990-2001 Available from: URL: http://www.wjgnet.com/1007-9327/full/v23/i11/1990.htm DOI: http://dx.doi.org/10.3748/wjg.v23.i11.1990

INTRODUCTION

Gastric cancer is the second leading cause of cancer-related death worldwide[1]. The prognosis of patients with advanced and unresectable gastric cancers is very poor with a median survival rate of approximately 10 mo[2]. Recently, fluorouracil and its derivatives, cisplatin, irinotecan, taxane and trastuzumab, have been recognized as first-line treatments for gastric cancer[2]. 5-Fluorouracil continuous infusion (5-FUci) is accepted as a standard chemotherapy regimen for advanced gastric cancer for its minimal toxicity as shown in clinical trials[2]. However, treatment responses vary in individual patients, mainly due to the heterogeneous and dynamic nature of tumor progression after sequential treatments. Thus, early detection and accurate assessment of tumor response to treatment is essential for individualized treatment planning[3].

Diffusion-weighted magnetic resonance imaging (DW-MRI) has emerged as a noninvasive imaging technique, which exploits tissue water mobility reflective of the microstructural properties of tumor tissue and detects tissue changes after treatment. DW-MRI uses motion-probing gradients to sensitize MRI signal loss arising from the Gaussian diffusion distribution. Higher tissue cellularity and cell membrane integrity of tumor malignancy are associated with more restricted diffusion, whereas tumor cell apoptosis and necrosis result in increased diffusivity of water molecules[4,5]. Tissue water mobility can be quantified by the apparent diffusion coefficient (ADC) using the conventional mono-exponential model to fit DW signals acquired at 2-3 b-values between 0 and 1000 s/mm^2. ADC primarily represents extracellular tissue diffusion with a mixed effect of fast diffusion component arising from microvascular blood flow. Previous studies have demonstrated that ADC values increase after chemotherapy, radiotherapy or administration of combined targeted medicine, indicating that ADC may serve as an imaging biomarker for the assessment of tissue microstructural changes prior to any changes in tumor size[6-8]. However, ADC values after treatment may not consistently increase because treatment may cause cellular swelling in the early phase of apoptosis

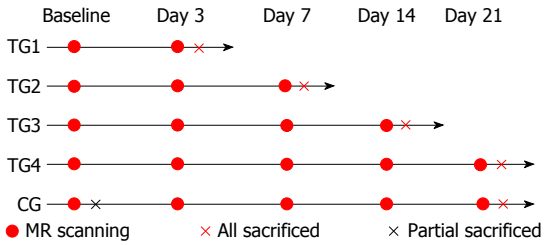

Figure 1 Schedule of magnetic resonance image acquisition and sacrifice of treated and control mice. TG: Treated group; CG: Control group.

and may cause the formation of fibrosis, both of which decrease the extracellular space and consequently decrease ADC values[6,8]. The complex interplay of biophysical processes including tissue cellularity, intracellular and extravascular/extracellular water diffusion, and tissue perfusion contributes to variations in post-treatment ADC values that have yet to be clarified[8].

With multiple b-values at lower range, the DW signal decay deviating from mono-exponential decay is not non-negligible due to the pseudo-perfusion effect at lower b-values. To more accurately evaluate post-treatment tumor tissue changes, extravascular diffusion and microvascular perfusion need to be distinguished from each other using an advanced DW-MRI method that takes into account the intravoxel incoherent motion (IVIM) phenomenon[9]. The IVIM DW-MRI may distinguish between multi-compartmental (*e.g.*, diffusion *vs* perfusion and intracellular *vs* extracellular) effects in biological tissues[9]. IVIM DW-MRI exploits the fact that, by using more diffusion weightings (b-values) at lower b-values (0-200 s/mm^2) with smaller intervals, DW signal decay can be used to quantify microvascular perfusion activity, whereas signal decay at higher b-values (> 200 s/mm^2) can be used to quantify tissue water molecular diffusion; therefore, IVIM DW-MRI can distinguish the microvascular perfusion effect from "pure" diffusion. Consequently, IVIM DW-MRI allows the following to be calculated noninvasively without contrast agent administration: the "pure" (slow) diffusion coefficient (D), pseudo-perfusion (fast) diffusion coefficient (D*), and fractional volume (f_p)[9,10]. IVIM measurements have been used to differentiate between benign and malignant tumors[11-13] and evaluate therapeutic responses to chemotherapy in different tumor types[14-17]. However, the variability of IVIM measurements in response to chemotherapy and/or radiotherapy in these studies remains controversial.

To the best of our knowledge, no previous studies have evaluated the therapeutic response to the standard chemotherapy 5-FU using IVIM DW-MRI in an animal model of gastric adenocarcinoma. The purpose of our study was to evaluate treatment response in tumor tissues by studying changes in diffusion and pseudo-perfusion properties based on ADC and IVIM measurements in a mouse model of gastric adenocarcinoma as early as 3 d after treatment, and to compare the imaging findings with histopathological results of tissue cellularity and microvascular properties at designated post-treatment time points.

MATERIALS AND METHODS

Animal model

All experimental procedures were approved by the Institutional Review Board of and Institutional Animal Care and Use Committee of Peking University People's Hospital, Beijing, China. Animals were housed in a pathogen-free facility at a temperature of 22 ℃, humidity of 61%, and a 12 h light–dark cycle. They were provided with food and water in accordance with the animal welfare guidelines established by our institution's Office of Laboratory Animal Welfare (OLAW). Twenty-seven BALB/c nude female mice, weighing 20-24 g and aged 6-8 wk, were obtained from the Vital River Laboratories (Beijing, China). They were acclimated to their new environment for one week before experimentation.

All animals were randomly divided into a control group (CG) and four treated groups (TG1-4) with five mice in each treated group and seven in the control group. All groups underwent MRI scans and were sacrificed for histopathological analysis based on the schedule shown in Figure 1. Two mice in the control group were sacrificed at baseline after MRI scanning. Five mice in the control group underwent MRI at each time point (day 0, day 3, day 7, day 14, and day 21) and were then sacrificed on day 21. All tumors were resected from each animal post-sacrifice for serial histopathological analyses and compared with the MRI findings.

Tumor model

Cells from the poorly differentiated human gastric adenocarcinoma cell line MKN-45 were obtained from the American Type Culture Collection (Rockville, MD, United States). MKN-45 cells were cultured in Dulbecco's modified Eagle's medium (DMEM) and supplemented with 10% fetal bovine serum and 1% nonessential amino acids. Concentrations of 95% O_2 and 5% CO_2 were maintained. Cells were passaged twice a week with a 1:2 split using 0.25% trypsin (HyClone, Ft. Collins, CO, United States). The tumor xenografts were developed by subcutaneously injecting approximately 1 × 10^6 cells suspended in 100 μL medium, into both flanks of the nude mice; therefore, each mouse developed two tumors. Tumors grew for 10-15 d until they reached 100-250 mm^3 in size prior to treatment.

Treatment protocol

Animals in the treated groups received 5-FU injections (40 mg/kg) (Shangdong Qilu Pharmaceutical Co., Ltd., China) in 0.2 mL 0.9% sodium chloride intraperitoneally

Table 1 Parameters of T2WI and intravoxel incoherent motion MR scanning

	T2WI	IVIM
Plane	Axial and coronal	Axial
TR (ms)	2800	2500
TE (ms)	72	42
Fat suppression	No	Yes
Matrix	256 × 192	64 × 64
FOV (mm^2)	70 × 35	70 × 35
Thickness (mm)	1.5	1.5
Gap (mm)	0.5	0.5
NEX	4	1 (b = 0-300) 2 (b = 400-600) 4 (b = 800-1500)
b value (s/mm^2)	NA	0, 10, 20, 30, 50, 80, 130, 200, 300, 400, 600, 800, 1000, and 1500

IVIM: Intravoxel incoherent motion.

once a day for 5 consecutive days starting on day 0. No medicine was given during the last two days of the week[18]. In addition, calcium folinate (Jiangsu Hengrui Medicine Co., Ltd., China) was injected (45 mg/kg) intraperitoneally twice a day; the first injection was given one hour before the 5-FU injection, and the second injection was given at the same time as the 5-FU injection. This procedure was repeated for three weeks. Animals in the control group received intraperitoneal injections of 0.1 mL sterile water at the same time points as the treated animals received 5-FU injections.

Image acquisition

MR images were acquired on a 3.0 Tesla MRI scanner (Discovery 750, GE Healthcare, Waukesha, WI, United States). Each mouse was anesthetized with an intraperitoneal injection of pentobarbital sodium (50 mg/kg). After anesthetization, the mouse was placed in a test tube filled with salt alginate impression gel. The gel had been dissolved in warm water before use to mitigate the possibility of artifacts arising from the tissue-air interface at each subcutaneous xenograft tumor area and to maintain the mouse's body temperature. The tube containing the mouse was then placed in a small animal birdcage coil (Magtron Inc., Jiangyin, China) in the supine position on the MR platform. Anatomic MR images for tumor volume measurements were acquired with a T2-weighted (T2W) spin-echo (SE) sequence with the parameters listed in Table 1.

DW-MR images were acquired with a single-shot SE echo-planar imaging (DW-SE-EPI) sequence with the parameters listed in Table 1. A spatial-spectral excitation pulse was used to excite a slice of magnetization from water protons while leaving the fat protons unaffected to achieve fat suppression. Parallel imaging using the array spatial-sensitivity encoding technique (ASSET) was employed to reduce the echo train length and thus mitigate image distortion. The total acquisition time for anatomic and DW-MRI scanning was approximately 15 min.

Post-processing

Anatomic and DW-MR images were transferred to a workstation (SW45; GE Healthcare, Waukesha, WI, United States). One radiologist with 5 years of experience in MRI interpretation performed tumor volume (V_T) measurements on the axial and coronal T2W MR images. He was blinded to the treatment conditions and histopathological results. The three-dimensional maximal diameters of each tumor were measured. Tumor volume was calculated as $4/3\pi \times$ (length × width × height)/2.

On each DW image slice with b-value = 0 s/mm^2, a region of interest (ROI) of the entire tumor was manually drawn and automatically copied onto DW images with other b-values. Within each ROI, the averaged signal intensity at each b-value was calculated. In the standard clinical protocol, conventional ADC was calculated by the linear fitting of the logarithm of signal intensities acquired at b-value = 0 and 1000 s/mm^2.

IVIM parameters, including the fast diffusion coefficient (D*) and corresponding fractional volume (V_{fast}), and the slow diffusion coefficient (D), and corresponding fractional volume (V_{slow}), were calculated using the bi-exponential model $S(b)/S(0) = V_{slow} \times e^{-bD} + V_{fast} \times e^{-b(D+D^*)}$ where $V_{fast} + V_{slow}$ approximately 1, and S(b) and S(0) represent the signal intensities at the corresponding b-value. The trust-region-reflective non-linear curve-fitting algorithm (Matlab, MathWorks Inc., Natick, MA, United States) was used for bi-exponential signal fitting to derive all four parameters. Prior to the non-linear fitting, the initial estimates of D and V_{slow} were derived by the linear fitting of DW signals with higher b-values (> 200 s/mm^2), where fast diffusion effects can be ignored. The initial estimate of D* was made by a linear fitting of signals with lower b-values (< 80 s/mm^2), where the fast diffusion effect dominated the signal decay. Finally, the fractional volume of the fast component that is presumably considered the pseudo-perfusion fractional volume (f_p) was calculated as $100\% \times V_{fast}/(V_{fast} + V_{slow})$. In order to compare the fitting behavior using the two-compartment bi-exponential IVIM and mono-exponential signal decay model, both methods were used to fit the signal decay with the full range of 14 b-values in a subset of animals.

Histopathological analysis

After image acquisition, animals in the treated groups and control group were sacrificed on day 3 (TG4), day 7 (TG3), day 14 (TG2), and day 21 (TG1 and CG). Two entire tumors from each sacrificed animal were excised, fixed in 10% formalin for 24 to 48 h, and immersed in 70% ethanol. Each tumor specimen was paraffin embedded and cut into 5-μm thick sections. Tissue sections were stained for immunohistochemistry on the Ventana Discovery XT Autostainer (Tucson, Arizona, United States). Immunohistochemical analyses including

Table 2 Median and interquartile range observed in intravoxel incoherent motion parameters, apparent diffusion coefficients and V_T values in the treated and control groups

		Day 0	Day 3	Day 7	Day 14	Day 21
V_T (mm^3)	Treated	219.96 (125.39-280.12)	356.88 (248.76-386.13)	368.33 (320.33-504.98)	559.3 (442.16-644.68)	439.7 (260.97-841.22)
	Control	157.1 (29.04-432.25)	281.71 (104.30-596.15)	476.34 (261.56-777.13)	938.64 (511.07-1345.82)	1515.24 (675.23-1856.48)
ADC (mm^2/s)	Treated	0.57 (0.56-0.59)	0.62 (0.60-0.64)	0.62 (0.58-0.69)	0.83 (0.75-0.94)	0.72 (0.64-0.86)
	Control	0.61 (0.56-0.68)	0.57 (0.52-0.67)	0.55 (0.50-0.70)	0.65 (0.54-0.83)	0.77 (0.59-1.11)
D* (mm^2/s)	Treated	1.99 (1.89-2.47)	1.4 (1.28-1.60)	1.58 (1.36-1.70)	1.68 (1.61-1.82)	1.68 (1.36-1.92)
	Control	2.07 (1.57-2.57)	2.23 (1.61-2.68)	1.97 (1.42-2.89)	2.25 (1.53-2.36)	1.81 (1.59-2.00)
fp (%)	Treated	19.15 (15.23-21.27)	32.90 (28.38-40.72)	37.19 (26.63-46.91)	49.95 (42.81-55.49)	42.56 (38.02-53.59)
	Control	22.38 (14.52-29.10)	22.98 (16.22-33.03)	22.47 (16.46-28.54)	27.87 (24.35-47.52)	40.2 (33.40-54.69)
D (mm^2/s)	Treated	0.39 (0.37-0.41)	0.34 (0.29-0.37)	0.33 (0.23-0.36)	0.33 (0.29-0.35)	0.32 (0.23-0.38)
	Control	0.40 (0.33-0.44)	0.41 (0.33-0.44)	0.39 (0.33-0.47)	0.39 (0.32-0.47)	0.35 (0.32-0.44)

IVIM: Intravoxel incoherent motion; ADC: Apparent diffusion coefficients.

Ki67, TUNEL and CD31 staining were performed on areas containing viable tumor tissues. Tumor cells, sufficiently stained with chromogen, were considered positive compared with the surrounding tissues. For each type of histopathological analysis, each stained slide was digitized with an optical magnification (× 200 or × 400) using a LEICA DFC 550 Digital Microscope Camera (Wetzlar, Germany). One pathologist (W.G.) with 10 years of experience defined the viable tumor areas by avoiding significant areas of necrosis on the slides. The microscopic images were then analyzed by Image J (version 1.42; National Institutes of Health, Bethesda, MD, United States) to automatically detect the difference between the target cells with positive staining and the background cells. The detected target cells were manually confirmed based on the image intensity and minimum particle size threshold[19]. At least three sections from each tumor were measured and averaged.

With regard to Ki67 staining (ab15580; Abcam, Cambridge Science Park, United Kingdom), the proliferating cell density was calculated as the ratio of cells stained by Ki-67 to the total number of background cells. In TUNEL staining (Roche, Basel, Switzerland), the apoptotic cell density was calculated as the ratio of cells with positive TUNEL expression to the total number of viable tumor cells. In CD31 staining (sc1506; Santa Cruz Biotechnology, Santa Cruz, CA, United States), microvessel endothelial cells were identified, and the microvessel density (MVD) was calculated as the total number of vessels divided by the viable tumor cells. In addition, each tumor section was stained with hematoxylin and eosin (H&E, Sigma-Aldrich; Ventana, Tucson, AZ, United States) to delineate tumor necrosis. The necrotic fraction was calculated as the ratio of the necrotic area to the total tumor area on at least three sections of each tumor; these ratios were then averaged.

Statistical analysis

The median and interquartile range of tumor volume (V_T), ADC, D, D*, and f_p were calculated for baseline and post-treatment scans. Medians were calculated due to the data skew distribution observed in the stem-leaf plot.

Median percentage changes (ΔV_T%, ΔADC%, ΔD*% and Δf_p%) between baseline and each post-treatment scan in each tumor were calculated. Logarithm transformation was used to meet the precondition of the normal distribution for mixed linear model analysis. After logarithm transformation, ΔV_T%, ΔADC%, ΔD*% and Δf_p% were compared between the control and treated groups using the mixed linear regression model with the restricted maximum likelihood method, and were recorded as z values. *P* values less than 0.05 were considered statistically significant. All statistical analyses were performed using the statistical software Stata (version 13.0; StataCorp LP, College Station, Texas, United States).

RESULTS

Two animals from TG2 and TG3 died on day 2 after treatment. One animal in TG1 was excluded due to severe ulceration on day 3 after treatment. Two animals from TG2 and TG3 were excluded due to severe image distortion and chemical shift artifacts present in IVIM DW images. After these exclusions, the mice were distributed throughout the study groups as follows: 7 (CG), 4 (TG1), 3 (TG2), 3 (TG3), and 5 (TG4).

Tumor volume measurement

Tumor volumes at baseline and at each post-treatment time point in the treated and control groups are shown in Table 2 and Figure 2A; percentage changes (ΔV_T%) in baseline and post-treatment time points were then calculated (Figure 3A). Differences in ΔV_T% between the treated group and the control group were not significantly different on day 3 ($\Delta V_{Ttreated}$% = 103% and $\Delta V_{Tcontrol}$% = 125%, z = -0.17, *P* = 0.8659) and day 7 ($\Delta V_{Ttreated}$% = 127% and $\Delta V_{Tcontrol}$% = 384%, z = -1.36, *P* = 0.1724). However, tumor volumes in the control group on day 14 ($\Delta V_{Tcontrol}$% = 890%) and day 21 ($\Delta V_{Tcontrol}$% = 1449%) were significantly higher than those in the treated group at the same time points ($\Delta V_{Ttreated}$% = 187%, z = -3.62,

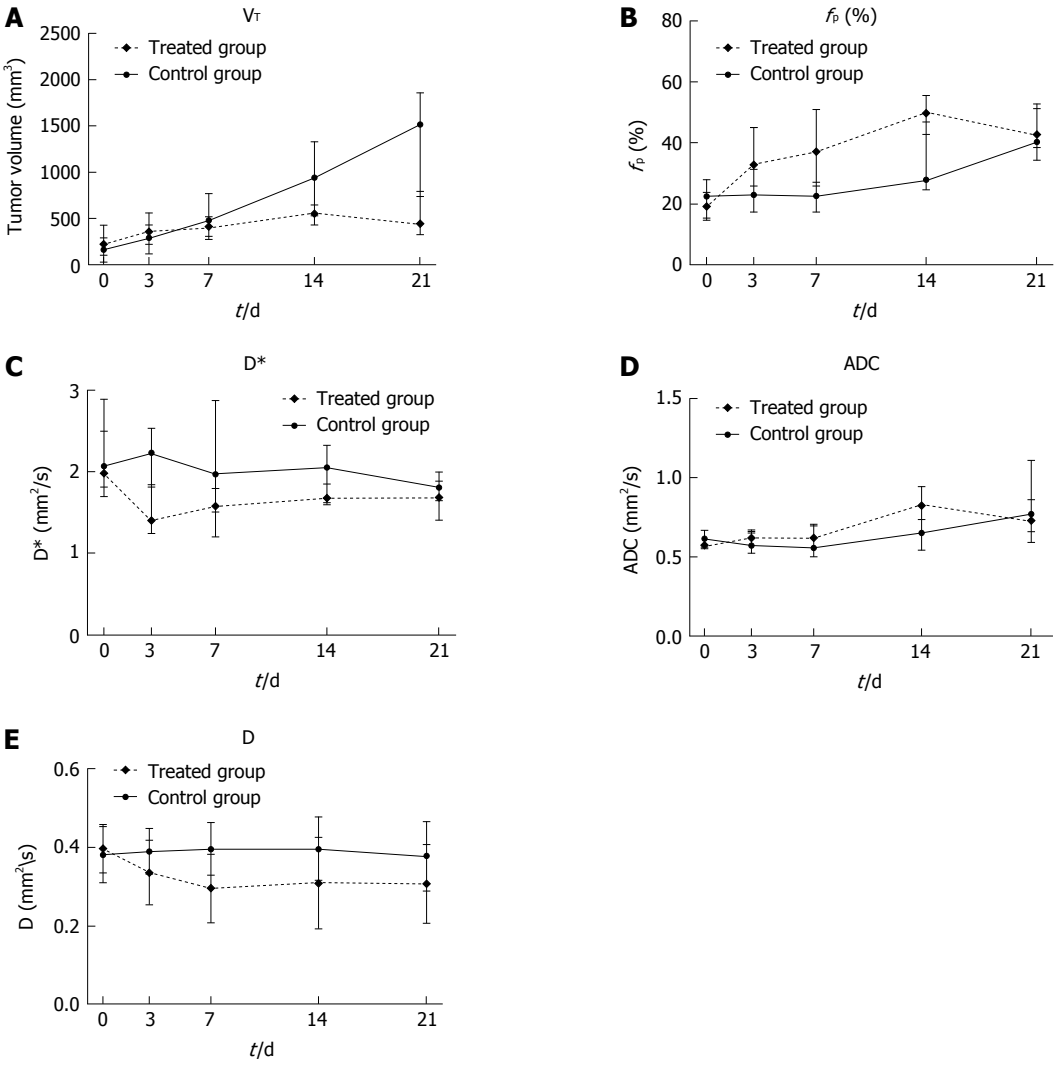

Figure 2 Median tumor volume (A), *fp* (B), D* (C), apparent diffusion coefficients (D) and D values (E) of all animals in the treated groups (dashed line) and control group (solid line). The vertical bars represent the interquartile ranges. ADC: Apparent diffusion coefficient.

P = 0.0003 and $\Delta V_{Ttreated}$% = 156%, z = -6.30, P = 0.0001), respectively. Tumor volume changes in two representative mice (treated and control) are shown on T2W images (Figure 4). Tumor volume in the control group increased significantly from day 14 to day 21, whereas no obvious tumor volume changes were observed in the treated group from day 3 to day 21.

Tumor IVIM measurement

IVIM measurements (D, D* and f_p) and conventional ADC values for all tumors in the treated and control groups at each time point are shown in Table 2 and Figure 2B-E. The median percentage changes in pre-treatment baseline and each post-treatment time point are shown in Figure 3B-D.

The IVIM derived perfusion measurements D* and f_p showed opposite trends with decreasing perfusion related diffusion coefficients (D*) and increasing perfusion fractions (f_p) after treatment. D* in the treated groups decreased on days 3, 7, 14, and 21 with a median percentage change ($\Delta D^*_{treated}$%) of -30%, -34%, -20% and -31%, respectively. In contrast, D* in the control group was close to baseline with a median percentage change ($\Delta D^*_{control}$%) of 3%, 1% and -1% on days 3, 7 and 14, which were significantly different from $\Delta D^*_{treated}$% at each time point (z = -5.40, -4.18 and -1.95, P = 0.0001, 0.0001 and 0.0244). D* in the control group decreased at the end of the experimental period on day 21 ($\Delta D^*_{control}$% = -9%), which was not significantly different from that in the treated group (z = -1.95, P = 0.0513). The median percentage increase in f_p in the treated groups ($\Delta f_{ptreated}$%) was as follows: 93% on day 3, 113% on day 7 and 181% on day 14, and the percentage change in f_p in the control group ($\Delta f_{pcontrol}$%) increased less during the course of the study (13%, 9% and 58% on days 3, 7 and 14). Significant differences in Δf_p% were found between the treated and control groups on day 3, 7 and 14 (z = 4.63, 5.52, and 2.12, P = 0.001, 0.0001, and 0.0336), respectively. At the end of the experimental period (day 21), the treated and control groups showed increases in f_p ($\Delta f_{ptreated}$%

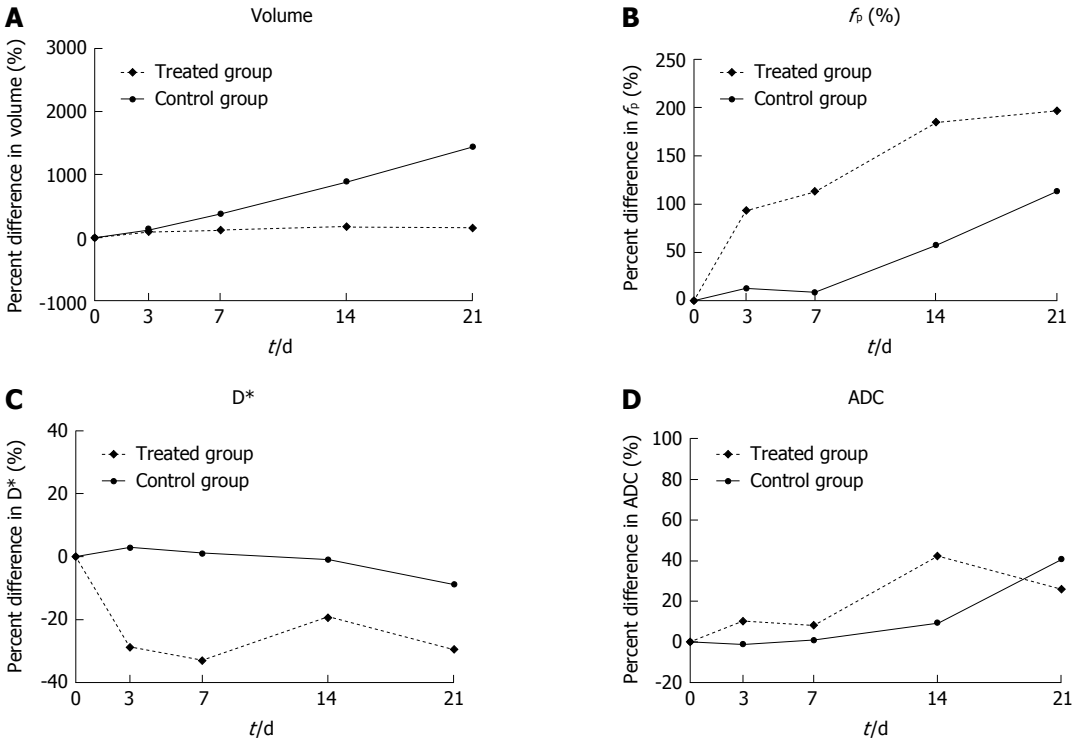

Figure 3 Median percentage change from baseline in tumor volume (A), *fp* (B), D* (C) and ADC (D) values of all animals in the treated groups (dashed line) and control group (solid line), $P < 0.01$.

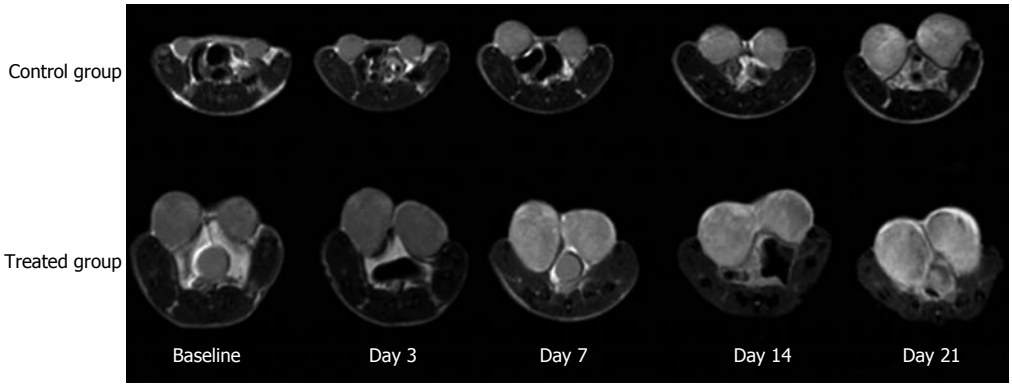

Figure 4 Representative axial T2-weighted images of a control mouse (first row) and a treated mouse (second row) before (baseline) and after treatment (day 3, day 7, day 14 and day 21). Tumor volumes in the control mouse markedly increased on day 14 and day 21. In comparison, tumor volume in the treated mouse did not show an obvious change after treatment.

= 179% and $\Delta f_{pcontrol}$% = 113%), but no significant differences were observed (z = 1.15, P = 0.2484).

The ADC value in the treated groups increased with median percentage changes ($\Delta ADC_{treated}$%) of 11%, 9%, 42%, and 26% on days 3, 7, 14 and 21 after treatment, whereas the ADC in the control group only increased slightly before day 14 ($\Delta ADC_{control}$% = -1%, 1% and 10% on days 3, 7 and 14, respectively), but with a marked increase of 41% on day 21. The difference in ΔADC% between the control and treated groups was significant on day 3 (z = 2.44, P = 0.0147) and day 14 (z = 2.40, P = 0.0164), but not on day 7 (z = 1.40, P = 0.1600) or day 21 (z = -0.10, P = 0.9213).

IVIMDW images and signal intensity decay with increasing b-values were observed in two representative mice in the control and treated group (Figure 5). Tumor areas were clearly delineated in the images without obvious artifacts. Tumor areas showed brighter signals due to more restricted tissue water diffusion compared to the surrounding tissues. The signal-to-noise ratio of the tumor ROI at the highest b value was beyond the background noise; therefore, it was sufficient for bi-exponential fitting (Figure 5B). Within each tumor ROI, DW signal decay was fitted more adequately with the bi-exponential model to calculate the IVIM-related parameters compared to the mono-exponential model (Figure 5B). Faster signal decay in the treated mouse indicated overall increased motion of water molecules

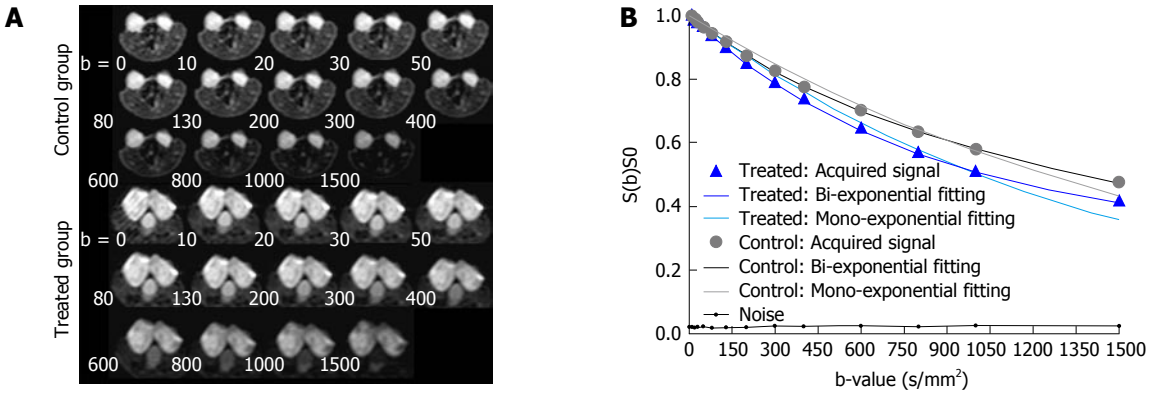

Figure 5 IVIMDW images and signal intensity decay with increasing b-values. A: IVIMDW images acquired at increasing b-values in a representative mouse from the treated group and one from the control group; B: Within the tumor ROI, the averaged signal intensity decay as a function of the b-value is plotted (day 7) by both the bi-exponential and mono-exponential model, respectively. For the treated mouse, D* = 1.27 × 10^{-3} mm^2/s, *fp* = 57.3% and ADC = 0.69 × 10^{-3} mm^2/s. For the control mouse, D* = 2.15 × 10^{-3} mm^2/s, *fp* = 17.2% and ADC = 0.55 × 10^{-3} mm^2/s.

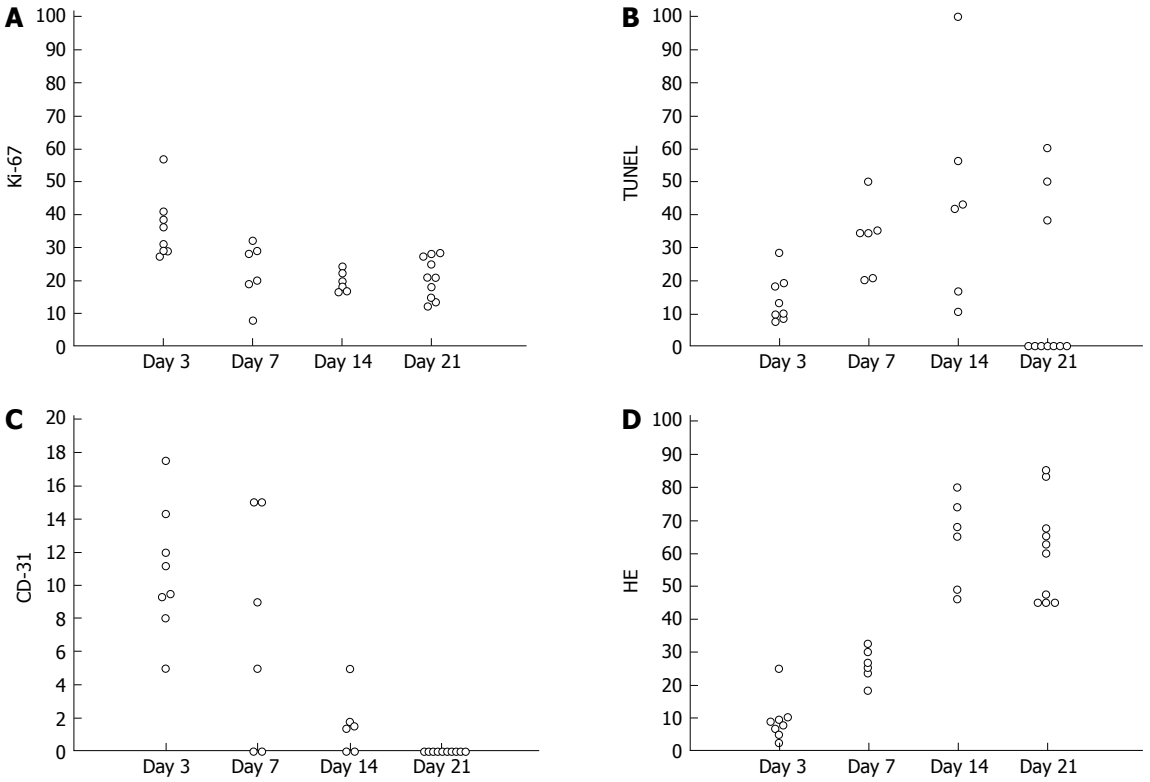

Figure 6 Change in histopathological examinations. A: Proliferating cell density (Ki67 staining); B: Apoptotic cell density (TUNEL staining); C: Microvessel density (CD31 staining); D: Necrosis fraction (HE staining), are plotted at each time point after treatment in the treated group.

and less organized tissue microstructure secondary to treatment.

Histopathological characteristics

The proliferating cells identified on Ki-67 staining showed an apparent decrease at each time point in the treated groups (Figure 6A). The apoptotic activity, quantified as the percentage of cells positive in TUNEL staining, demonstrated a marked increase after treatment (Figure 6B). Vascularity of the endothelium assessed by CD31 staining demonstrated a trend toward reduced MVD after treatment (Figure 6C). The tumor necrotic fraction identified by H&E staining increased markedly after treatment (Figure 6D). In tumor tissues replaced by significant necrosis during the treatment course, non-positive cells were identified in histopathological analyses and are labeled as 0 in Figure 6. Representative histopathological images (Ki-67, TUNEL, CD31 and H&E) of the treated animals revealed tumor tissue changes at each time point during treatment (Figure 7). At the end of the experimental period (day 21), extensive areas of tumor

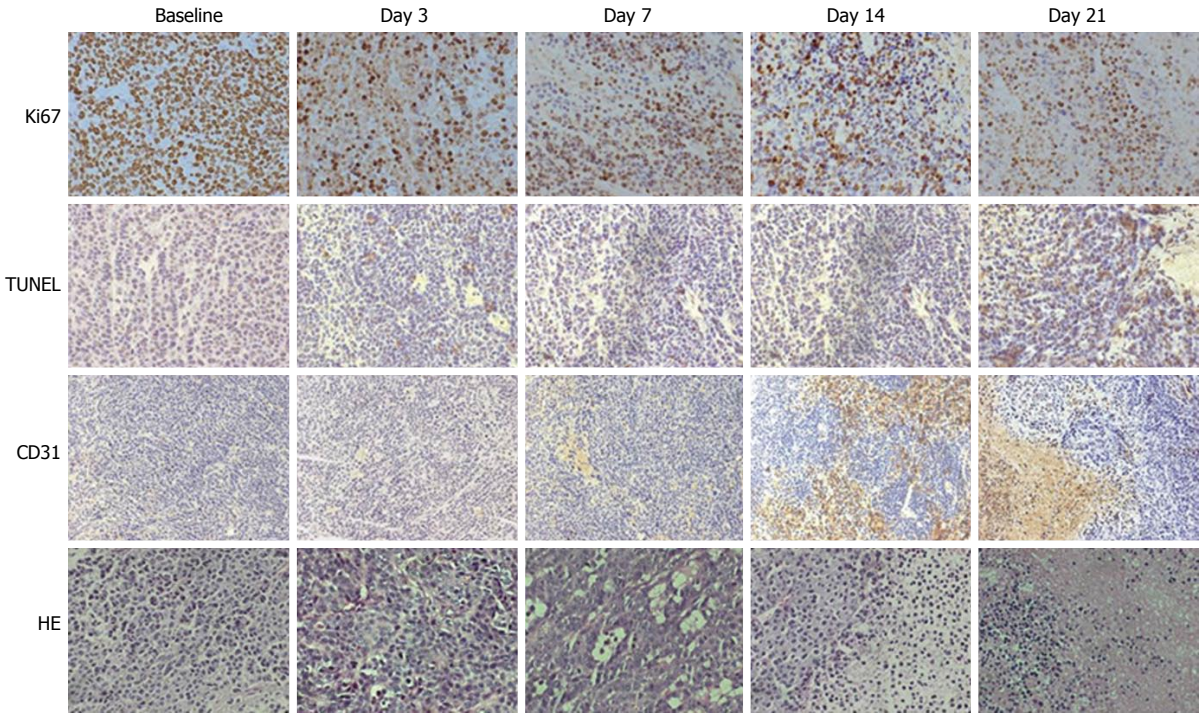

Figure 7 Representative histopathological images of a tumor specimen with Ki-67 staining (first row), TUNEL staining (second row), CD31 staining (third row) and hematoxylin and eosin staining (fourth row) at baseline, day 3, day 7, day 14 and day 21 after treatment in the treated group. Brown staining in the Ki-67 images indicates cells in the proliferative state. Brown staining in the TUNEL images indicates cells undergoing apoptosis. Brown staining in the CD31 images indicates endothelial cells. Viable tumor tissues and necrosis were identified on HE stainings. HE: Hematoxylin and eosin.

necrosis were present in both treated and control mice.

DISCUSSION

In the present DW-MRI study, we found significant changes in the fast diffusion coefficient (D*) and fractional volume (f_p) as early as three days after chemotherapy in a mouse model of gastric adenocarcinoma based on the bi-exponential IVIM model. We demonstrated that IVIM parameters provide critical information in addition to conventional apparent diffusion measurement for the assessment of treatment response. DW-MRI findings correlated well with histopathological changes showing a decrease in proliferating cells and MVD and an increase in apoptosis and tumor necrosis in the treated group.

The IVIM model developed by Le Bihan[8,20] suggests that at the macroscopic level, the capillary network is distributed in space in a pseudorandom manner, and the overall movement of the blood's water molecules within capillaries (*i.e.*, perfusion) mimics the diffusion model. The perfusion-related fast diffusion coefficient D* is considered proportional to the mean capillary segment length and average blood velocity[20]. As reported in previous studies, D* can be used to distinguish benign and malignant salivary gland tumors based on the fact that angiogenesis in malignant tumors leads to increased microscopic blood flow[13]. IVIM DW-MRI has also been used in previous clinical studies to investigate therapeutic responses in different tumor types. Lewin *et al*[17] demonstrated that f_p increased two weeks after treatment of advanced hepatocellular carcinoma with the anti-angiogenic drug sorafenib, whereas changes in the pure diffusion coefficient D and ADC values were not significant. Hauser *et al*[15] evaluated the therapeutic response to radiotherapy combined with chemotherapy and/or targeted therapy with cetuximab in patients with squamous cell carcinomas of the head and neck. Significant increases in f_p, D, and ADC values at 7.5 mo after therapy were demonstrated in patients based on standard clinical progression evaluation criteria. Ganten *et al*[14] reported an increase in D values at week 2 and 4 after treatment with no change in f_p in a rectal cancer study. However, in the aforementioned clinical treatment response assessment studies, a change in D* in response to treatment was not reported. A recent experimental study reported that D* significantly decreased only 4 h after treatment, but recovered to baseline at 24 h in a rabbit VX2 liver tumor model treated with the vascular disrupting agent CKD-516[9]. The variability of IVIM derived measurements in these studies may be attributed to inconsistent IVIM imaging protocols, the range of b-values, and multi-compartment diffusion signal models[4,9].

In our study, we found that D* decreased significantly after treatment, which significantly correlated with decreased MVD revealed by endothelial cell CD31 staining. In addition, increased cellular apoptosis and necrosis in response to treatment may contribute

to changes in both tissue diffusion and perfusion properties. As a consequence, the destruction of tumor microvasculature and decreased cellularity led to the mixture of a fast perfusion component and a slow diffusion component after chemotherapy, which potentially resulted in an increased f_p approaching 50% and indicated equilibrium between perfusion and diffusion components. In contrast, D* was similar to the baseline value, and f_p showed a smaller increase in untreated tumors in the control group.

ADC derived from conventional DW MRI has been widely accepted for evaluating the therapeutic efficacy of chemotherapy, radiotherapy or combined therapy with targeted agents. Consistent with previous studies[19,21,22], our study showed that ADC values increased on day 3 after treatment, while tumor volumes in the treated groups remained stable during the entire treatment period, which indicated that microstructural tumor tissue changes precede changes in tumor size. However, the complex interplay of decreased cell proliferation, increased apoptosis and necrosis, and the destruction of tumor microvasculature may contribute to the variations in ADC after treatment[4,21]. As shown in our study, considerable overlap in ADC was observed between the treated and control groups at each time point after treatment. In comparison, no significant overlap in f_p and D* measurements were observed between the control and treated groups, which provided a more reliable assessment of tumor tissue changes.

At the end of the treatment cycle (day 21), all measurements were similar between the treated and control groups. H&E staining showed that viable tumor tissues were mostly replaced by tumor necrosis, which was induced by chemotherapy in the treated groups or due to progressive growth in the control group. In addition, CD31 staining only identified a few endothelial cells in tumor microvasculature in both the control and treated groups on day 21, indicating the destruction of microvasculature.

The slow diffusion coefficient (D) is generally considered the pure diffusion coefficient describing extracellular and extravascular tissue water mobility[1,3,8]. We observed significant decreases in D (most D values were very close to 0) from day 7 to day 21 after treatment, which did not match the findings of previous studies[14,15]. For this reason, we did not calculate the percentage changes in D values at each time point further as we did with the other IVIM parameters shown in the results. Our explanation for this finding is that D in the two-compartment model may not represent real physiological changes, but may be a covariate parameter in the process of iterative converges of the nonlinear bi-exponential signal fitting. As discussed above, destruction of the tumor microenvironment after chemotherapy leads to a mixture of perfusion and diffusion components and thus can cause a deviation from the assumption of bi-exponential signal decay. Therefore, the term $V_{slow} \times e^{-bD}$ may become a constant term, meaning that D will need to decrease to a very small number so that the signal decay begins to follow a mono-exponential model. In this situation, the resultant D values may not reflect true physiological changes when it reaches a number close to zero. In order to measure more robust slow diffusion coefficients, we performed linear fitting of the logarithm DW signal decay with b-value = 200 and 1500 s/mm^2, where the perfusion effect can be ignored. We found that the slow diffusion coefficient derived from linear fitting of the high b-value DW signals increased after treatment (data not shown), similar to the ADC changes.

This study had some limitations. First, the sample size in each treated group was relatively small. Second, the bi-exponential IVIM-DWI model was the only model used to characterize the complicated tissue water mobility. There are several sophisticated diffusion models that have been investigated for multi-b-value signal fitting, such as the stretched exponential model, the diffusion kurtosis model, and the fractional order calculus (FROC) model[16,17]. The stretched model yields the intravoxel diffusion heterogeneity index and distributed diffusion coefficient. Similarly, the FROC model describes the anomalous diffusion process and yields a new set of parameters including the fractional order derivative in space (β) and a spatial parameter (μ). The value of β is mathematically equivalent to the heterogeneity index generated by the stretched model. We also used the FROC model to fit the diffusion decay; however, the changes in both β and μ were not stable and did not show differences between the treated and control groups during the course of the study (data not shown).

In addition, a recent study[23] suggested that although these sophisticated models may provide more information on tissue water diffusion, their biologic interpretation requires further refinement and they are not directly correlated with pathological characteristics. In contrast, our calculations based on the bi-exponential model were based on the theory that it might allow separation of water molecular diffusion from the microcirculation. Our results demonstrated that the fast diffusion coefficient and fractional volume provided valuable information reflective of tissue microvasculature changes secondary to chemotherapy and correlated well with each specific pathological finding. Interestingly, a recent study[24] compared a DW signal fitting plot using all these diffusion models, which clearly demonstrated that the bi-exponential model had the best fit of the signal decay with b < 1500 s/mm^2. Finally, the bi-exponential model was considered to be the most appropriate model for this study. Nonetheless, all of these diffusion models should be investigated further to compare their respective accuracies regarding tumor characterization and treatment response in future studies.

The present study demonstrated that the IVIM-derived tissue perfusion related diffusion coefficient and fraction parameters provided valuable information reflective of tissue microstructural and microvasculature

changes secondary to chemotherapy. The fast diffusion coefficient (D*) decreased, whereas the fast diffusion fractional volume (f_p) increased immediately after treatment and throughout the treatment course. ADC increased in both the treated and control groups with greater increases in the treated groups. No significant overlaps were observed in D* and f_p measurements between the treated and control groups, whereas ADC showed more overlap.

In conclusion, IVIM perfusion measurements offer a potentially accurate evaluation of chemotherapy efficacy and may facilitate individualized treatment planning and prompt treatment adjustment in gastric cancer patients.

ACKNOWLEDGMENTS

The authors would like to express their sincere thanks to Samantha Schoeneman (Manager of Medical Editing and Writing, iCoreMed Technology and Service LLC), and Kelly Bauer (Editor, iCoreMed Technology and Service LLC) who conducted a linguistic revision of this manuscript.

COMMENTS

Background

Early detection and accurate assessment of tumor response to chemotherapy is essential for individualized treatment planning in patients with gastric cancer.

Research frontiers

In a mouse gastric cancer model, the authors demonstrated that the intravoxel incoherent motion (IVIM)-derived tissue perfusion coefficient (D*) decreased, whereas the perfusion fraction (PF) increased immediately after chemotherapy and throughout the treatment course.

Innovations and breakthroughs

No significant overlaps were observed in D* and PF measurements between the treated and control groups; such overlaps were observed using the conventional apparent diffusion coefficient measurements.

Applications

IVIM-derived perfusion measurements offer the potential of accurate evaluation of chemotherapeutic efficacy. This imaging study is ready to be translated into a clinical study that may facilitate individualized treatment planning and prompt treatment adjustment in gastric cancer patients.

Terminology

The IVIM model developed by Le Bihan suggests that at the macroscopic level, the capillary network is distributed in space in a pseudorandom manner, and the overall movement of the blood's water molecules within capillaries (*i.e.*, perfusion) mimics the diffusion model. Consequently, IVIM diffusion-weighted magnetic resonance imaging (DW-MRI) allows the following to be calculated noninvasively without contrast agent administration: the "pure" (slow) diffusion coefficient (D), the pseudo-perfusion (fast) diffusion coefficient (D*), and the fractional volume (f_p).

Peer-review

DW-MRI has emerged as a noninvasive imaging method, which exploits tissue water mobility reflective of the microstructural properties of tumor tissue and detects tissue changes after treatment. It was the aim of the authors to exploit IVIM-DW-MRI with a biexponential model for chemotherapy response evaluation in a gastric cancer mouse model. The authors demonstrated that in a mouse gastric cancer model the IVIM-derived tissue perfusion coefficient (D*) decreased whereas the PF increased immediately after chemotherapy and throughout the treatment course as well.

REFERENCES

1 **Ferlay J**, Shin HR, Bray F, Forman D, Mathers C, Parkin DM. Estimates of worldwide burden of cancer in 2008: GLOBOCAN 2008. *Int J Cancer* 2010; **127**: 2893-2917 [PMID: 21351269 DOI: 10.1002/ijc.25516]

2 **Louvet C**, André T, Tigaud JM, Gamelin E, Douillard JY, Brunet R, François E, Jacob JH, Levoir D, Taamma A, Rougier P, Cvitkovic E, de Gramont A. Phase II study of oxaliplatin, fluorouracil, and folinic acid in locally advanced or metastatic gastric cancer patients. *J Clin Oncol* 2002; **20**: 4543-4548 [PMID: 12454110]

3 **Jain RK**, Duda DG, Willett CG, Sahani DV, Zhu AX, Loeffler JS, Batchelor TT, Sorensen AG. Biomarkers of response and resistance to antiangiogenic therapy. *Nat Rev Clin Oncol* 2009; **6**: 327-338 [PMID: 19483739 DOI: 10.1038/nrclinonc.2009.63]

4 **Padhani AR**, Liu G, Koh DM, Chenevert TL, Thoeny HC, Takahara T, Dzik-Jurasz A, Ross BD, Van Cauteren M, Collins D, Hammoud DA, Rustin GJ, Taouli B, Choyke PL. Diffusion-weighted magnetic resonance imaging as a cancer biomarker: consensus and recommendations. *Neoplasia* 2009; **11**: 102-125 [PMID: 19186405]

5 **Koh DM**, Collins DJ. Diffusion-weighted MRI in the body: applications and challenges in oncology. *AJR Am J Roentgenol* 2007; **188**: 1622-1635 [PMID: 17515386 DOI: 10.2214/AJR.06.1403]

6 **Hamstra DA**, Rehemtulla A, Ross BD. Diffusion magnetic resonance imaging: a biomarker for treatment response in oncology. *J Clin Oncol* 2007; **25**: 4104-4109 [PMID: 17827460 DOI: 10.1200/JCO.2007.11.9610]

7 **Loveless ME**, Lawson D, Collins M, Nadella MV, Reimer C, Huszar D, Halliday J, Waterton JC, Gore JC, Yankeelov TE. Comparisons of the efficacy of a Jak1/2 inhibitor (AZD1480) with a VEGF signaling inhibitor (cediranib) and sham treatments in mouse tumors using DCE-MRI, DW-MRI, and histology. *Neoplasia* 2012; **14**: 54-64 [PMID: 22355274]

8 **Thoeny HC**, De Keyzer F, Vandecaveye V, Chen F, Sun X, Bosmans H, Hermans R, Verbeken EK, Boesch C, Marchal G, Landuyt W, Ni Y. Effect of vascular targeting agent in rat tumor model: dynamic contrast-enhanced versus diffusion-weighted MR imaging. *Radiology* 2005; **237**: 492-499 [PMID: 16192323 DOI: 10.1148/radiol.2372041638]

9 **Le Bihan D**, Breton E, Lallemand D, Aubin ML, Vignaud J, Laval-Jeantet M. Separation of diffusion and perfusion in intravoxel incoherent motion MR imaging. *Radiology* 1988; **168**: 497-505 [PMID: 3393671 DOI: 10.1148/radiology.168.2.3393671]

10 **Le Bihan DJ**. Differentiation of benign versus pathologic compression fractures with diffusion-weighted MR imaging: a closer step toward the "holy grail" of tissue characterization? *Radiology* 1998; **207**: 305-307 [PMID: 9577472 DOI: 10.1148/radiology.207.2.9577472]

11 **Doblas S**, Wagner M, Leitao HS, Daire JL, Sinkus R, Vilgrain V, Van Beers BE. Determination of malignancy and characterization of hepatic tumor type with diffusion-weighted magnetic resonance imaging: comparison of apparent diffusion coefficient and intravoxel incoherent motion-derived measurements. *Invest Radiol* 2013; **48**: 722-728 [PMID: 23669588 DOI: 10.1097/RLI.0b013e3182915912]

12 **Orsi G**, Aradi M, Nagy SA, Perlaki G, Trauninger A, Bogner P, Janszky J, Illés Z, Dóczi T, Pfund Z, Schwarcz A. Differentiating white matter lesions in multiple sclerosis and migraine using monoexponential and biexponential diffusion measurements. *J Magn Reson Imaging* 2015; **41**: 676-683 [PMID: 24677284 DOI: 10.1002/jmri.24580]

13 **Talbot CB**, Lagarto J, Warren S, Neil MA, French PM, Dunsby C. Correction Approach for Delta Function Convolution Model Fitting of Fluorescence Decay Data in the Case of a Monoexponential

Reference Fluorophore. *J Fluoresc* 2015; **25**: 1169-1182 [PMID: 26063535 DOI: 10.1007/s10895-015-1583-4]
14 **Ganten MK**, Schuessler M, Bäuerle T, Muenter M, Schlemmer HP, Jensen A, Brand K, Dueck M, Dinkel J, Kopp-Schneider A, Fritzsche K, Stieltjes B. The role of perfusion effects in monitoring of chemoradiotherapy of rectal carcinoma using diffusion-weighted imaging. *Cancer Imaging* 2013; **13**: 548-556 [PMID: 24334520 DOI: 10.1102/1470-7330.2013.0045]
15 **Hauser T**, Essig M, Jensen A, Gerigk L, Laun FB, Münter M, Simon D, Stieltjes B. Characterization and therapy monitoring of head and neck carcinomas using diffusion-imaging-based intravoxel incoherent motion parameters-preliminary results. *Neuroradiology* 2013; **55**: 527-536 [PMID: 23417120 DOI: 10.1007/s00234-013-1154-9]
16 **Karaman MM**, Sui Y, Wang H, Magin RL, Li Y, Zhou XJ. Differentiating low- and high-grade pediatric brain tumors using a continuous-time random-walk diffusion model at high b-values. *Magn Reson Med* 2016; **76**: 1149-1157 [PMID: 26519663 DOI: 10.1002/mrm.26012]
17 **Lewin M**, Fartoux L, Vignaud A, Arrivé L, Menu Y, Rosmorduc O. The diffusion-weighted imaging perfusion fraction f is a potential marker of sorafenib treatment in advanced hepatocellular carcinoma: a pilot study. *Eur Radiol* 2011; **21**: 281-290 [PMID: 20683597 DOI: 10.1007/s00330-010-1914-4]
18 **Bras-Gonçalves RA**, Pocard M, Formento JL, Poirson-Bichat F, De Pinieux G, Pandrea I, Arvelo F, Ronco G, Villa P, Coquelle A, Milano G, Lesuffleur T, Dutrillaux B, Poupon MF. Synergistic efficacy of 3n-butyrate and 5-fluorouracil in human colorectal cancer xenografts via modulation of DNA synthesis. *Gastroenterology* 2001; **120**: 874-888 [PMID: 11231942]
19 **Kim H**, Morgan DE, Zeng H, Grizzle WE, Warram JM, Stockard CR, Wang D, Zinn KR. Breast tumor xenografts: diffusion-weighted MR imaging to assess early therapy with novel apoptosis-inducing anti-DR5 antibody. *Radiology* 2008; **248**: 844-851 [PMID: 18710978 DOI: 10.1148/radiol.2483071740]
20 **Dixon WT**. Separation of diffusion and perfusion in intravoxel incoherent motion MR imaging: a modest proposal with tremendous potential. *Radiology* 1988; **168**: 566-567 [PMID: 3393682 DOI: 10.1148/radiology.168.2.3393682]
21 **Thoeny HC**, Ross BD. Predicting and monitoring cancer treatment response with diffusion-weighted MRI. *J Magn Reson Imaging* 2010; **32**: 2-16 [PMID: 20575076 DOI: 10.1002/jmri.22167]
22 **Wybranski C**, Zeile M, Löwenthal D, Fischbach F, Pech M, Röhl FW, Gademann G, Ricke J, Dudeck O. Value of diffusion weighted MR imaging as an early surrogate parameter for evaluation of tumor response to high-dose-rate brachytherapy of colorectal liver metastases. *Radiat Oncol* 2011; **6**: 43 [PMID: 21524305 DOI: 10.1186/1748-717X-6-43]
23 **Sui Y**, Wang H, Liu G, Damen FW, Wanamaker C, Li Y, Zhou XJ. Differentiation of Low- and High-Grade Pediatric Brain Tumors with High b-Value Diffusion-weighted MR Imaging and a Fractional Order Calculus Model. *Radiology* 2015; **277**: 489-496 [PMID: 26035586 DOI: 10.1148/radiol.2015142156]
24 **Bai Y**, Lin Y, Tian J, Shi D, Cheng J, Haacke EM, Hong X, Ma B, Zhou J, Wang M. Grading of Gliomas by Using Monoexponential, Biexponential, and Stretched Exponential Diffusion-weighted MR Imaging and Diffusion Kurtosis MR Imaging. *Radiology* 2016; **278**: 496-504 [PMID: 26230975 DOI: 10.1148/radiol.2015142173]

P- Reviewer: Fang BL, Shivapurkar N **S- Editor**: Qi Y
L- Editor: Ma JY **E- Editor**: Zhang FF

Published by **Baishideng Publishing Group Inc**
8226 Regency Drive, Pleasanton, CA 94588, USA
Telephone: +1-925-223-8242
Fax: +1-925-223-8243
E-mail: bpgoffice@wjgnet.com
Help Desk: http://www.wjgnet.com/esps/helpdesk.aspx
http://www.wjgnet.com

ISSN 1007-9327